JOURNAL OF AIRCRAFT
Vol. 40, No. 3, May–June 2003

Aileron Buzz Simulation Using an Implicit Multiblock Aeroelastic Solver

Guowei Yang* and Shigeru Obayashi†
Tohoku University, Sendai 980-8577, Japan
and
Jiro Nakamichi‡
National Aerospace Laboratory, Tokyo 181-0015, Japan

A fully implicit multiblock aeroelastic solver, which coupled thin-layer Navier–Stokes equations with structural equations of motion, has been developed for the flutter simulation on complex aerodynamic configurations. Navier–Stokes equations are solved with a lower–upper symmetric Gauss–Seidel subiteration algorithm and a modified Harten–Lax–van Leer–Einfeldt–Wada scheme. Structural equations of motion are discretized by a direct second-order differential method with subiteration in generalized coordinates. The transfinite interpolation is used for the grid deformation of the blocks neighboring the flexible surface. To evaluate the effectiveness of the grid deformation, a comparison is first done for the oscillating LANN wing with a rigidly attached grid and a deforming grid. Then the method is applied to predict the flutter speed and frequency of the AGARD 445.6 standard aeroelastic wing. Finally, the aeroelastic instability referred to as aileron buzz is simulated for the supersonic transport model of the National Aerospace Laboratory of Japan.

I. Introduction

THE National Aerospace Laboratory (NAL) of Japan has established a research program for scaled experimental supersonic airplanes for five years. A nonpowered experimental airplane will be launched in 2002 by a solid rocket booster.[1] Because thin wing sections and control surfaces are necessarily used for high-speed aircraft for aerodynamic performance, it is important to predict accurately the transonic nonlinear aeroelastic phenomena such as flutter, buffet, and aileron buzz for the structural design of aircraft.

In the last decade, transonic nonlinear aeroelastic analyses have been extensively studied by solving Euler/Navier–Stokes equations coupled with the structural equations of motion.[2–5] However, in these methods, the flow governing equations are only loosely coupled with the structural equations of motion, namely, after the aerodynamic loads are determined by solving the flow governing equations, the structural model is used to update the position of the body. The coupling contains an error of one time step; thus, these methods are always only first-order accurate in time regardless of the temporal accuracy of the individual solvers of the flow and structural equations.

The tightly coupled aeroelastic approach was first put forward by Alonso and Jameson[6] for a two-dimensional Euler aeroelastic simulation, called the dual-time implicit–explicit method. In each real time step, the time-accurate solution is solved by the explicit Runge–Kutta time-marching method for a steady problem, so that all of the convergence acceleration techniques, such as multigrid, residual averaging, and local time step, can be implemented in the calculation. In general, about 100 pseudotime steps are needed for the explicit iterations to ensure adequate convergence; thus, the method is still very time consuming. In sofar as the authors know, only three-dimensional Euler results have been reported recently.[7] Goura et al.[8] constructed a first-order implicit time-marching scheme, as well as an only first-order implicit spatial discretization for the solution of a pseudosteady flow. Second-order temporal and spatial accuracy can be maintained as pseudosteady flow convergence. Euler equations were chosen as the aerodynamic governing equations due to the limitation of computational time.

Melville et al.[9] proposed a fully implicit aeroelastic solver between the fluids and structures, in which a second-order approximate factorization scheme with subiterations was performed for the flow governing equations, and the structural equations were cast in an iterative form. Because the restricted number of iterations cannot remove sequencing effects and factorization errors completely at every time step, a relatively small time step was used in their calculation. Nevertheless, a fully implicit aeroelastic Navier–Stokes solver with three subiterations has succeeded in the flutter simulation for an aeroelastic wing.[10]

In the flutter calculation, due to the deformation of the aeroelastic configuration, an adaptive dynamic grid needs to be generated at each time step. At present, most of aeroelastic calculations are only done for an isolated wing with single-block grid topology. For simple flexible geometry, the grid can be completely regenerated with an algebraic method[2] or a simple grid-deformation approach.[10] For complicated aerodynamic configurations, multiblock grids are usually generated for steady flow simulation. However, for an aeroelastic application, it is impossible to regenerate multiblock grids at each time step due to the limitation of computational cost. Multiblock grid-deformation approachs need to be used. Recently, Potsdam and Guruswamy[11] put forward a multiblock moving grid approach, which uses a blending method of a surface spline approximation and the nearest surface point movement for block boundaries, and transfinite interpolation (TFI) for the volume grid deformation. Wong et al.[12] also established a multiblock moving mesh algorithm. The spring network approach is utilized only to determine the motion of the corner points of the blocks, and the TFI method is applied to the edge, surface, and volume grid deformations.

In addition, structural data may be provided with the plate model, but the flow calculations are carried out for the full geometry. Interpolation between fluid and structure grids is required. Infinite

Received 5 March 2002; revision received 8 August 2002; accepted for publication 15 August 2002.

*Guest Researcher, Institute of Fluid Science, 2-1-1 Katahira; currently Associate Professor, Department of Mechanics and Mechanical Engineering, University of Science and Technology of China, Hefei, Anhui 230026, P.R. China, on leave.

†Associate Professor, Institute of Fluid Science, 2-1-1 Katahira. Associate Fellow AIAA.

‡Head, Aeroelasticity Group, Structures and Materials Research Center, 6-13-1 Osawa, Mitaka. Associate Fellow AIAA.

and finite surface splines,[13,14] developed for plate aerodynamics and plate structural models are still the main interpolation tools; however, the aerodynamic grid needs to be projected on the surface of the structural grid before interpolation. Goura et al.[15] recently suggested an interpolation method of constant volume transformation for the data exchange between fluids and structures based on the local grid information.

In the present paper, a fully implicit multiblock Navier–Stokes aeroelastic solver was developed based on the single-block aeroelastic code implemented previously.[16] The purpose of the present work is to simulate the aeroelastic phenomenon of aileron buzz on the supersonic transport (SST) designed by the NAL of Japan. First, the multiblock grid-deformation technique was assessed for a pitching oscillating wing with a rigidly attached grid and a deforming grid. Then, the flutter boundaries and frequencies for the AGARD 445.6 standard aeroelastic wing were predicted and compared with experimental data to validate the developed aeroelastic code. Finally, the aileron buzz cases were computed.

II. Governing Equations

Aerodynamic Governing Equations

In the paper, freestream density, freestream velocity, and the root chord or mean aerodynamic chord length are chosen as character quantities. Aerodynamic governing equations are the unsteady, three-dimensional, thin-layer Navier–Stokes equations in strong conservation law form, which can be written in curvilinear space ξ, η, ζ, and τ in nondimensional form as

$$\partial_\tau \hat{Q} + \partial_\xi F + \partial_\eta G + \partial_\zeta H = Re^{-1}\partial_\zeta H_v + S_{\mathrm{GCL}} \tag{1}$$

In the formulation, the viscosity coefficient μ in H_v is computed as the sum of laminar and turbulent viscosity coefficients, which are evaluated by Sutherland's law and the Baldwin–Lomax model with the Degani–Schiff modification. For multiblock grid calculation, the turbulence model is difficult to apply to the blocks with no solid surface because the model needs not only the local flowfield but also its corresponding gradient values on the wall surface. In addition, the thin-layer approximation may be unsuitable for general multiblock grids in which one block may have more than two solid surfaces. Therefore, the multiblock grids are carefully generated to have a single solid surface.

The source term S_{GCL} in Eq. (1) is obtained from the geometric conservation law[17] for a moving mesh, which is defined as

$$S_{\mathrm{GCL}} = Q\left\lfloor \partial_t J^{-1} + (\xi_t/J)_\xi + (\eta_t/J)_\eta + (\zeta_t/J)_\zeta \right\rfloor \tag{2}$$

Structural Dynamic Governing Equations

Second-order linear structural dynamic governing equations after normalization similar to the flow governing equation can be written as

$$[M]\{\ddot{d}\} + [K]\{d\} = \{F\} \tag{3}$$

where $[M]$ and $[K]$ are the nondimensional mass and stiffness matrices, respectively, and $\{F\}$ and $\{d\}$ are the aerodynamic load and displacement vectors, respectively. To solve Eq. (3), the Rayleigh–Ritz method is used. For a specific aerodynamic configuration, the natural mode shapes and frequencies can be calculated by finite element analysis or obtained from experimental influence coefficient measurements. In this study, the data of natural mode shapes and frequencies are calculated by finite element analysis. In general, only the first N modes, are considered. With these first N modes, we have an approximate decription of the displacement vector of the system given by

$$\{d\} = [\Phi]\{q\} \tag{4}$$

Because the natural modes are orthogonal with respect to both the mass and stiffness matrices, premultiplying Eq. (3) by $[\Phi]^T$ yields structural equations in generalized coordinates,

$$\ddot{q}_i + 2\zeta_i\omega_i\dot{q}_i + \omega_i^2 q_i = [\Phi]_i^T F \big/ M_i \tag{5}$$

where

$$\omega_i^2 = [\Phi]_i^T\{K\}[\Phi], \qquad M_i = [\Phi]_i^T\{M\}[\Phi]$$

The modal damping is readily added on the left-hand side of Eq. (5), where ζ_i is the damping ratio in the ith mode. The equation can be written as a first-order system by defining $S = [q, \dot{q}]$:

$$\dot{S} + \begin{bmatrix} 0 & -1 \\ \omega_i^2 & 2\omega_i\varsigma_i \end{bmatrix} S = \begin{bmatrix} 0 \\ [\Phi]_i^T F \big/ M_i \end{bmatrix} \tag{6}$$

III. Numerical Method

The lower–upper symmetric Gauss–Seidel (LU-SGS) method of Yoon and Jameson,[18] which employs a Newton-like subiteration, is used to solve Eq. (1). Second-order temporal accuracy is obtained by utilizing a three-point backward difference in the subiteration procedure. The numerical algorithm can be deduced as

$$\begin{aligned} LD^{-1}U\Delta Q = -\phi^i\big\{&(1+\phi)Q^p - (1+2\phi)Q^n + \phi Q^{n-1} \\ &- J\Delta\tau Q^p[(\xi_t/J)_\xi + (\eta_t/J)_\eta + (\zeta_t/J)_\zeta]^p \\ &+ J\Delta\tau\left[\delta_\xi F^p + \delta_\eta G^p + \delta_\zeta\left(H^p - H_v^p\right)\right]\big\} \end{aligned} \tag{7}$$

where

$$L = \bar{\rho}I + \phi^i J\Delta\tau\left(A^+_{i-1,j,k} + B^+_{i,j-1,k} + C^+_{i,j,k-1}\right), \qquad D = \bar{\rho}I$$

$$U = \bar{\rho}I - \phi^i J\Delta\tau\left(A^-_{i+1,j,k} + B^-_{i,j+1,k} + C^-_{i,j,k+1}\right)$$

$$\bar{\rho} = 1 + \phi^i J\Delta\tau(\bar{\rho}(A) + \bar{\rho}(B) + \bar{\rho}(C))$$

$$\phi^i = 1/(1+\phi), \qquad \Delta Q = Q^{p+1} - Q^p$$

Here, $\phi = 0.5$, and p is the subiteration number. The deduced subiteration scheme reverts to the standard LU-SGS scheme for $\phi = 0$ and $p = 1$. In fact, regardless of the temporal accuracy of the left-hand side of Eq. (7), second-order time accuracy is maintained when the subiteration number tends to infinity.

The inviscid terms in Eq. (7) are approximated by the modified third-order upwind Harten–Lax–van Leer–Einfeldt–Wada (HLLEW) scheme of Obayashi and Guruswamy.[19] For the isentropic flow, the scheme results in the standard upwind-biased flux-difference splitting scheme of Roe, and as the jump in entropy becomes large in the flow, the scheme turns into the standard HLLEW scheme. The thin-layer viscous term in Eq. (7) is discretized by second-order central differencing.

In the multiblock-grid method, the Navier–Stokes equations are solved in each block separately. The calculations of convective and viscous fluxes at block boundaries need flowfield values of two grid points in abutting blocks, and so the lagged flowfield always exists due to the lagged block boundary condition. When the LU-SGS method is used in the forward sweep, the correction of conserved variables ΔQ in the first-level halo cell is usually neglected. In the backward sweep, the correction of temporary variables $\Delta Q'$ obtained from the forward sweep can only be set to zero at block boundaries, which can produce a larger error than the same code using a single-block grid. Rizzetta and Visbal[20] consider that the subiteration can eliminate errors from linearization, factorization, lagged boundary conditions, and lagged turbulence models.

The structural equations of motion in generalized coordinates of Eq. (7) is discretized by a second-order scheme with subiterations of Ref. 10 as

$$\begin{aligned} &\begin{bmatrix} 1 & -\phi^i\Delta\tau \\ \phi^i\Delta\tau\omega_i^2 & 1 + 2\phi^i\omega_i\zeta_i\Delta\tau \end{bmatrix}\Delta S \\ &\quad = -\phi^i\left\{(1+\phi)S^p - (1+2\phi)S^n + \phi S^{n-1}\right. \\ &\qquad \left. + \Delta\tau\begin{bmatrix} 0 & -1 \\ \omega_i^2 & 2\omega_i\zeta_i \end{bmatrix}S^p - \Delta\tau\begin{bmatrix} 0 \\ [\Phi]_i^T F^p \big/ M_i \end{bmatrix}\right\} \end{aligned} \tag{8}$$

where $\Delta S = S^{p+1} - S^p$.

As $p \to \infty$, a fully implicit second-order temporal accuracy scheme for aeroelastic computation is formed by the coupling solutions of Eqs. (7) and (8). For accurate multiblock grid aeroelastic calculation, the subiteration method is very important not only for eliminating the lagged flowfield induced by lagged multiblock boundary condition but also for removing the sequencing effects between fluids and structures. However, in practical application, only finite subiterations can be used. For example, an approximately factored implicit solver with three subiterations was used in Ref. 10. Similarly, three subiterations are used for the present calculation. Because the restricted number of iterations does not remove sequencing effects and factorization errors at every time step completely, a proper time-step size needs to be evaluated by numerical tests.

IV. Multiblock Grid Generation and Deformation

Multiblock Grid Generation

For a complex aerodynamic configuration, multiblock grid generation continuously challenges the computational fluid dynamics community. Grid topology may be further limited due to the assumption of the thin-layer approximation and the use of turbulence model. However, for the aeroelastic application of the SST wing/fuselage model, an H-type multiblock grid with 30 blocks shown in Fig. 1 can be chosen to satisfy the requirements. The whole process to generate the grid is composed of four steps.

1) The surface grid is first distributed as shown in Fig. 2, which contains four zones, three zones for fuselage and one zone for the wing. A total eight zones are distributed on the whole surface of SST. Aileron surface is distributed at 12×13 grid points in the span- and chordwise directions, respectively.

2) The edge grids of each block are then generated with a polynomial function, which is determined by the coordinates and direction derivatives of two endpoints of the edge grid line.

3) The surface and volume grids of each block are generated sequentially with the two- and three dimensional TFI methods. The coefficients of interpolation are calculated with a robust set of blending functions proposed by Soni.[21]

4) Two- and three-dimensional elliptic methods with the forcing function control of Higenstock[22] are applied to smooth surface and volume grid distributions, to adjust the orthogonality at boundaries and to keep grid continuity between abutting blocks.

For the H-type multiblock grid, an acceptable grid can be generated only with the first three steps.

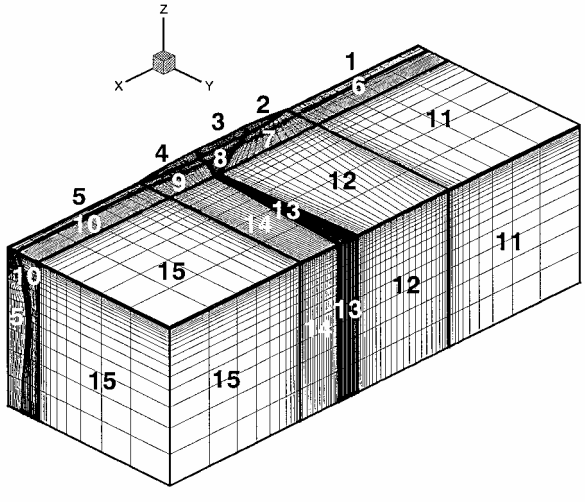

Fig. 1 Multiblock grid with 30 blocks for SST.

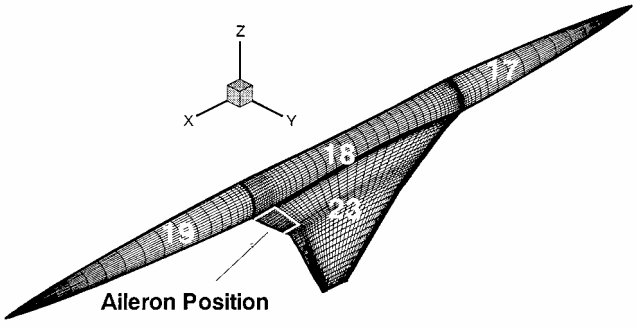

Fig. 2 Surface grid distribution on SST.

Multiblock Grid Deformation

For the described H-type multiblock grid topology with 30 blocks, the blocks containing the fuselage surface and the blocks away from the flexible wing can be fixed. Grid deformations only need be performed for the 12 blocks adjacent to the deforming wing. The computational cost for the grid deformation can be decreased greatly.

The TFI method[12] is applied to deform the grid blocks. Based on the known deformations of the flexible body and the parameterized arc-length values of the original grid, one-, two-, and three-dimensional TFI methods can be used to interpolate deformation values in the inner grid points. Then the deformations are added to the original grid to obtain the new multiblock grid. For the small and moderate aeroelastic deformations, the present method maintains the grid quality of the original grid and maximizes the reusability of the original grid. For the aileron deflection, a simple sheared mesh is used, and a gap is introduced between the ends of the aileron and wing to allow sufficient space for the moving sheared mesh. The present solver assumes the aileron oscillation of small amplitude. For aileron flutter analyses, the tendency of flow stability can be analyzed from the dynamic response of the aileron at a relatively small magnitude.

V. Data Transformation

In the present aeroelastic calculations, the structural modal data are provided with the plate model, and only normal deformation is considered. However, the real geometry is used for the fluid solution. Then the problem of passing information between the fluid and structural grids becomes very complicated. The fluid grid is first projected to the surface of structural grid. The deformations on the projected fluid grid points are interpolated by the infinite plate spline (IPS).[13] The new geometry can then be obtained by adding the deformations in the normal direction to the old geometry.

IPS is used to obtain an analytic function $w(x, y)$, which passes through the given structural deflections of N points $w_i = w(x_i, y_i)$. The static equilibrium equation of $D\nabla^4 w = q$ should be satisfied, where D is the plate elastic coefficient and q is the distributed load on the plate. The solution by superposition of fundamental functions can be written as

$$w(x, y) = a_0 + a_1 x + a_2 y + \sum_{i=1}^{N} F_i r_i^2 \ln r_i^2 \qquad (9)$$

where $r_i^2 = (x - x_i)^2 + (y - y_i)^2$.

The $N + 3$ coefficients of $(a_0, a_1, a_3, F_1, F_2, \ldots, F_N)$ in Eqs. (9) can be solved through the function passes, the given structural deflections of N and three additional conditions of the conservation of total force and moment:

$$\sum_{i=1}^{N} F_i = 0, \qquad \sum_{i=1}^{N} x_i F_i = 0, \qquad \sum_{i=1}^{N} y_i F_i = 0 \qquad (10)$$

Then the deformations of the aerodynamic grid points can be evaluated with function (9). The preceding linear displacement transformation can be written in the form $\delta S_a = [G]\delta S_s$, where δS_a and δS_s are the displacement vectors defined on the aerodynamic grid and the structural grid, respectively.

The force transformation from the fluid to the structural grids can be calculated with the principle of virtual work of $F_s = [G]^T F_a$, where F_s and F_a represent the forces on the structural and fluid grids, respectively. The principle of virtual work can guarantee the conservation of energy between the fluid and structural systems.

In the practical application, the LU decompositions of the coefficients matrix and its transpose matrix of the groups of Eqs. (9) and (10), with $a_0, a_1, a_3, F_1, \ldots, F_N$ as unknown quantities, are precalculated and stored in the code. For the flutter simulation of aileron oscillation on the SST, interpolations are applied on the aileron and wing separately because deformation is discontinuous between the zones of the aileron and wing.

VI. Results and Discussions

AGRAD LANN Wing

First, the three-dimensional periodic flows over the pitching LANN wing[23] are simulated with the deforming grid and the rigidly attached grid. The wing is defined by a linear interpolation between a supercritical airfoil at the root and another at the tip section, the airfoil thickness is about 12%, and the wing is twisted from 2.6 deg at the root section to −2 deg at the tip section. The wing has an aspect ratio of 7.92, a taper ratio of 0.4, and a quarter chord swept angle of 25 deg. The LANN wing oscillated around an unswept axis at 62.1% of the root chord in a pitch motion as

$$\alpha(t) = \alpha_m + \alpha_0 \sin(2kt) \tag{11}$$

where $\alpha_m = 0.6$ deg is the mean angle of attack, $\alpha_0 = 0.25$ deg is the amplitude of the oscillation, and $k = c\omega/2V_\infty = 0.102$ is the reduced frequency. The freestream Mach number is $M_\infty = 0.82$, and the Reynolds number based on root chord length is $Re = 7.3 \times 10^6$.

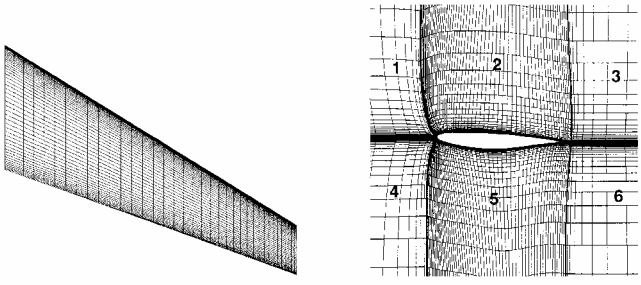

Fig. 3 Surface and H-type root sectional grids for LANN wing.

Instead of a single-block grid, a multiblock grid is generated in H-type topology for the wing shown in Fig. 3 to verify the multiblock grid-deformation method, which distributes $61 \times 39 \times 43$ grid lines in the chordwise, spanwise, and normal directions in the blocks containing the upper and lower surfaces of the wing, respectively. The grid line off the surface is about 10^{-5} root chord length. The number of total grid cells is 420,000. In the present multiblock Navier–Stokes solver, the block interface between abutting blocks requires one-to-one grid correspondence, and no block surface can contain wall surface and inner boundaries simultaneously. For the H-type multiblock grid, at least 12 blocks are needed, in which 6 blocks are located in the chordwise direction over the wing surface and another 6 are located beyond the wing tip.

For the attached grid method, the grid is only rotated with the rigid motion of the wing at each time step. The volume of grid cells are conserved unchanged and can be precalculated and stored in the code. The transformation derivatives can be calculated based on the initial values of ξ_{0x}, ξ_{0y}, and ξ_{0z} and the pitching motion rule of Eq. (11) as

$$\xi_x = \xi_{0x}\cos(\Delta\alpha) + \xi_{0z}\sin(\Delta\alpha), \qquad \xi_y = \xi_{0y}$$
$$\xi_z = -\xi_{0x}\sin(\Delta\alpha) + \xi_{0z}\cos(\Delta\alpha) \tag{12}$$

where $\Delta\alpha$ is the increment of the angle of attack. The grid speeds of inner grid points can also be calculated as $x_t = \alpha' z$ and $z_t = -\alpha' x$.

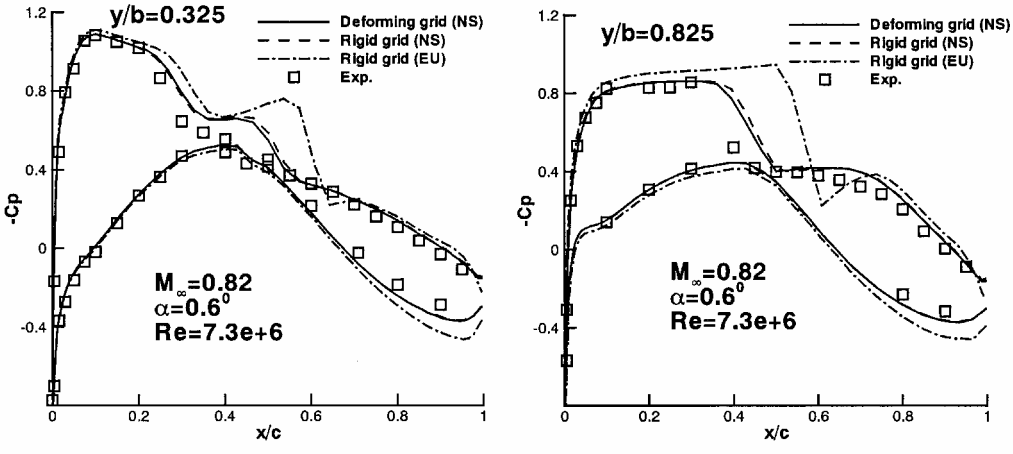

Fig. 4 Comparison of mean pressure coefficients for pitching LANN wing.

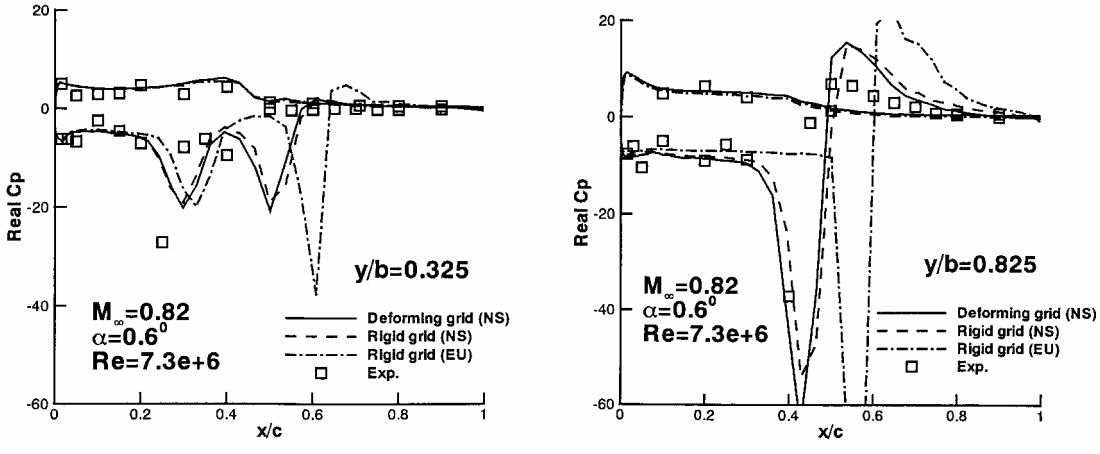

Fig. 5 Comparison of unsteady pressure in real part for pitching LANN wing.

However, for the deforming grid method, the grid is obtained by the grid of last time step added deformations interpolated with the grid-deformation method. The volume of grid cells is changeable in time, and the relations of Eq. 12 are not satisfied again. The transformed derivatives and the volume of grid cells need to be recalculated at each time step. The source term S_{GCL} must be considered in the calculation. The grid speeds at the $n+1$ time step can only be calculated from

$$x_t = \frac{3x^{n+1} - 4x^n + x^{n-1}}{2\Delta t} \tag{13}$$

The grid data of n and $n-1$ time steps had to be stored at each time step.

In the calculation, 2000 time steps are used to resolve the flow of one period, and three subiterations are added to eliminate various errors. Because solutions show periodicity after two periods, the calculated results are taken from the results of the third period. Figures 4–6 show the unsteady pressures obtained from the two methods compared with experimental data. The inviscid results are also shown in Figs. 4–6 to reflect the effect of viscosity. The main flow feature is a double shock that appears on the upper surface. When compared with experimental data, the Euler calculation predicts the shock 20% downstream and larger rear loading. The viscous results obtained from the deforming and rigid grids also agree with each other as well as predicts the slightly rear shock position.

AGARD 445.6 Wing

An aeroelastic wind-tunnel experiment is intrinsically destructive and, hence, much more expensive than a similar rigid-body experiment. Therefore, it is hard to find suitable experimental data to validate the developed aeroelastic solver. The unique complete aeroelastic experiment is available for the AGARD 445.6 standard aeroelastic wing,[24] which has been used to validate flutter simulations in several publications. The disadvantage of the test is that the nonlinear character is relatively weak due to a thin wing, and thus, linear, Euler, and Navier–Stokes equations all can predict good results when comparing with experimental data. However, in the absence of a better experiment, the experiment is still used to evaluate the current method.

The AGARD 445.6 wing model[24] was constructed of laminated mahogany and was essentially homogeneous. The wing has an aspect ratio 1.6525, a taper ratio of 0.6576, a quarter-chord swept angle of 45 deg, and a NACA 65A004 airfoil section. The number of grid points of the baseline grid is the same as in the LANN wing.

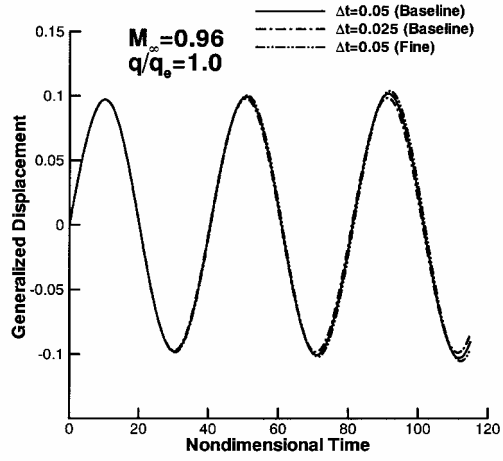

Fig. 8 Effect of grid and time-step sizes on the response of the first mode at $M_\infty = 0.96$ and $q/q_e = 1.0$.

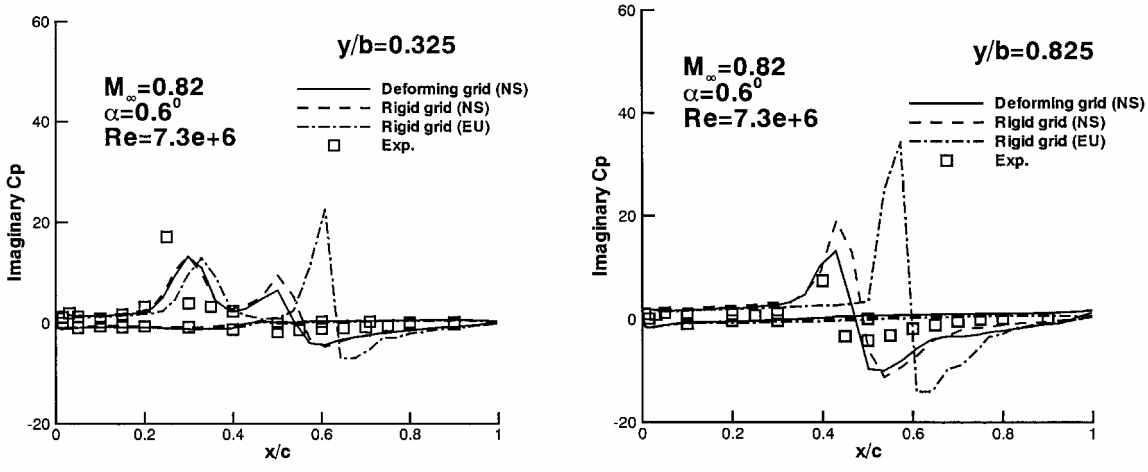

Fig. 6 Comparison of unsteady pressure in imaginary part for pitching LANN wing.

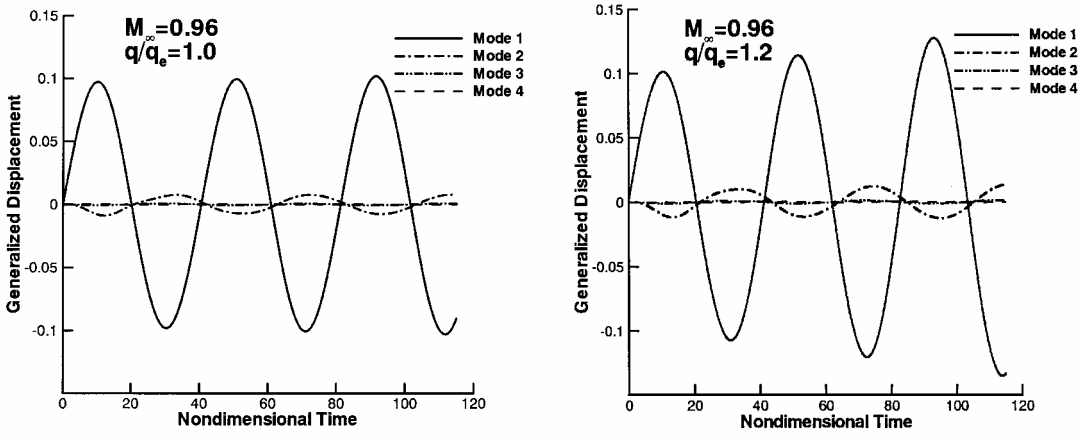

Fig. 7 Dynamic response of first four modes: $M_\infty = 0.96$ and $q/q_e = 1.0$ and 1.2.

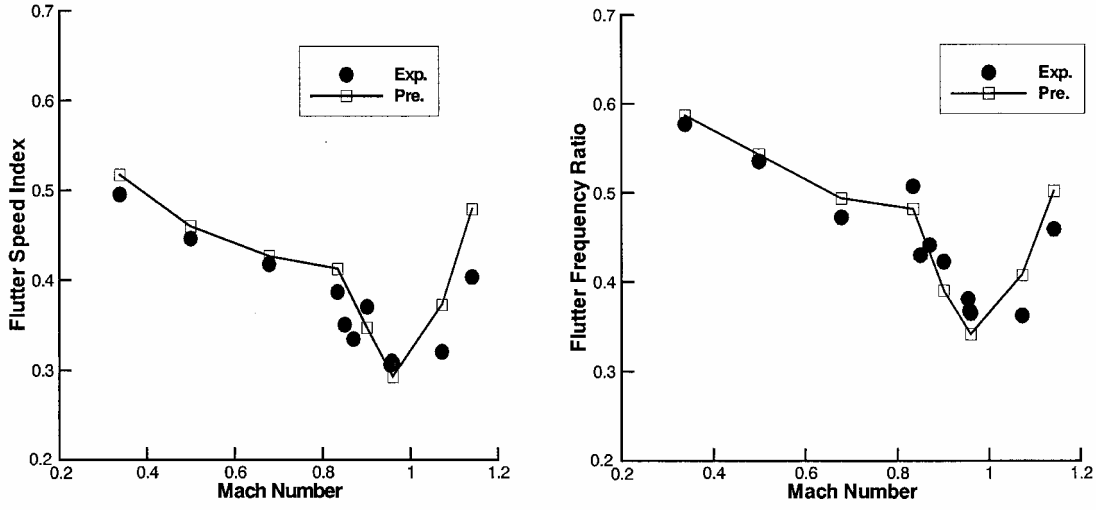

Fig. 9 Flutter speed and frequency for the AGARD 445.6 wing.

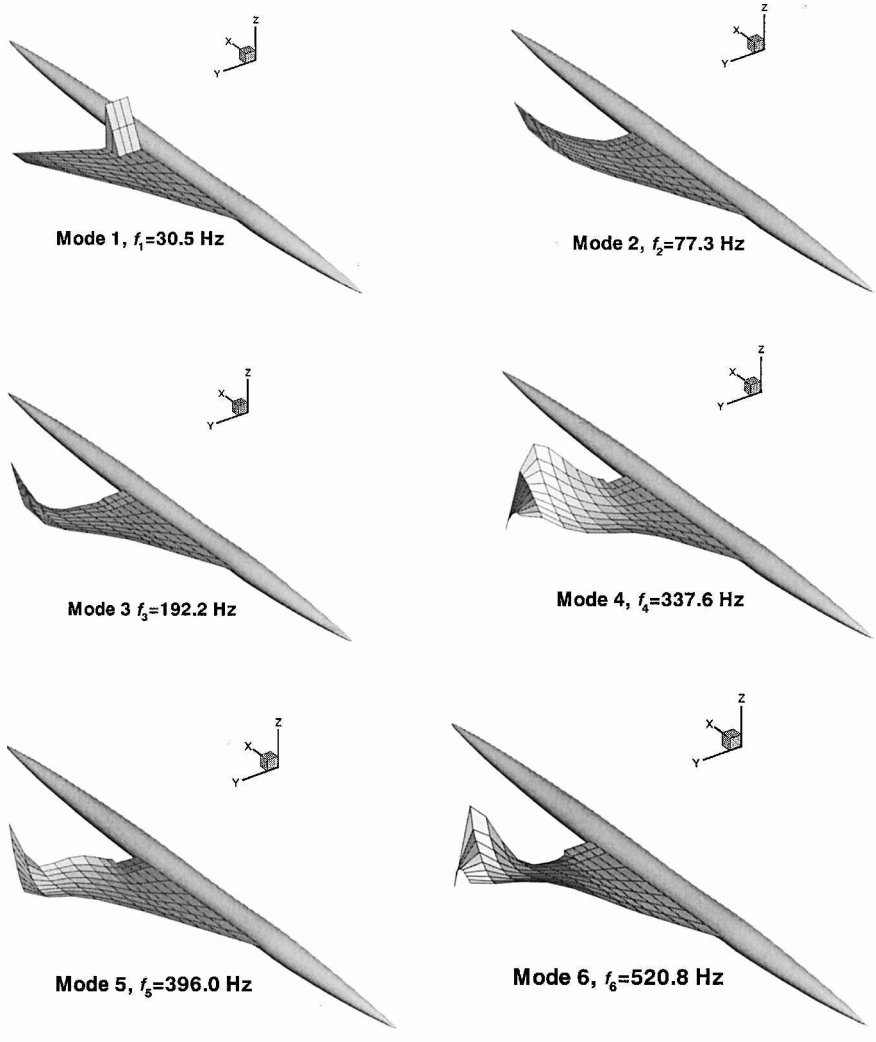

Fig. 10 First six modes and natural frequencies for SST weakened structural model.

To study the grid resolution, a fine grid is also generated, which mainly refines the grid blocks containing the upper and lower surfaces, namely, 20 grid points are added both in the chord and normal directions of the wing. The number of total grid cells of the refined grid is 744,000.

The first four structural modes and natural frequencies provided in Ref. 24 are used for the present computations, and a nondimensional time step is taken as $\Delta t = 0.05$ unless otherwise stated. All simulations are started from its corresponding steady flow. Each Mach number is run for several dynamic pressures to determine the flutter point. As the dynamic pressure is varied, the freestream density and Mach number are held fixed and Reynolds number is allowed to vary. At $t = 0$, a small initial velocity pertubation of 0.0001 for the first bending mode is applied to the wing.

The responses of the first four modes are shown in Fig. 7 for the $M_\infty = 0.96$ case at dynamic pressures $q/q_e = 1.0$ and 1.2, where the

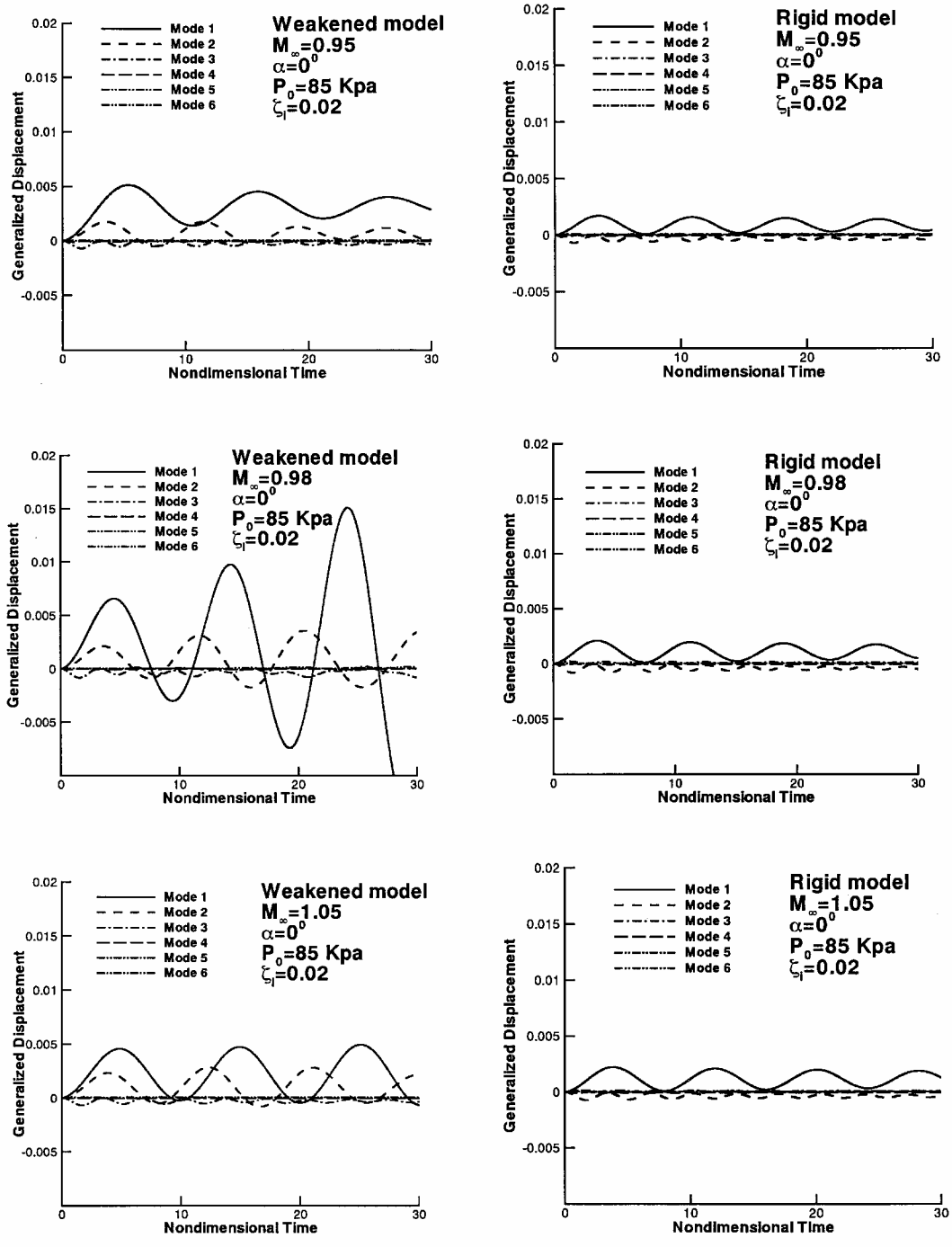

Fig. 11 Dynamic responses of first six modes for SST weakened and rigid structural models.

experimental flutter dynamic pressure is $q_e = 61.3$ lbf/ft^2. The dominant mode appears to be the first bending mode, and only the second mode has some effects on the first mode. The amplification factor of the first bending mode is analyzed, which is defined as the ratio of the magnitude of a peak to the magnitude of the previous peak of the same sign. Its corresponding response frequency is determined from the period between these two peaks. For the two cases, the amplifications and response frequencies are $AF = 1.023$ and $\omega = 84.135$ rad/s for $q/q_e = 1.0$ and $AF = 1.093$ and $\omega = 89.559$ rad/s for $q/q_e = 1.2$. Then the dynamic pressure and frequency for flutter ($AF = 1.0$) can be interpolated linearly as $q/q_e = 0.934$ and $\omega = 82.353$ rad/s.

The effect of the size of the time step and grid resolution on the response of the first bending mode for $q/q_e = 1$ is demonstrated in Fig. 8. Although independence of the grid and time step has not been achieved, only small differences exist by taking a half time step or using the fine grid. To compromise computational efficiency and accuracy, the present choice of time-step size and grid is appropriate. With the method, the flutter boundary and frequency over the Mach number range of 0.338–1.141 are calculated and compared with experimental data in Fig. 9. The typical transonic dip phenomenon is well captured. In the subsonic and transonic range, the calculated flutter speeds and frequencies agree well with experimental data; however, in the supersonic range, the present calculation overpredicts the experimental flutter points similar to other computations. To investigate the possible sources for the difference between the experiment and computation, Gordiner and Melville[10] examined the effects of various computational parameters, using 14 modes in the structural model, using different numerical schemes, and changing the location of the computational transition location downstream from the leading edge to the 30% chord location. However, only minimal effects of these changes were observed in the

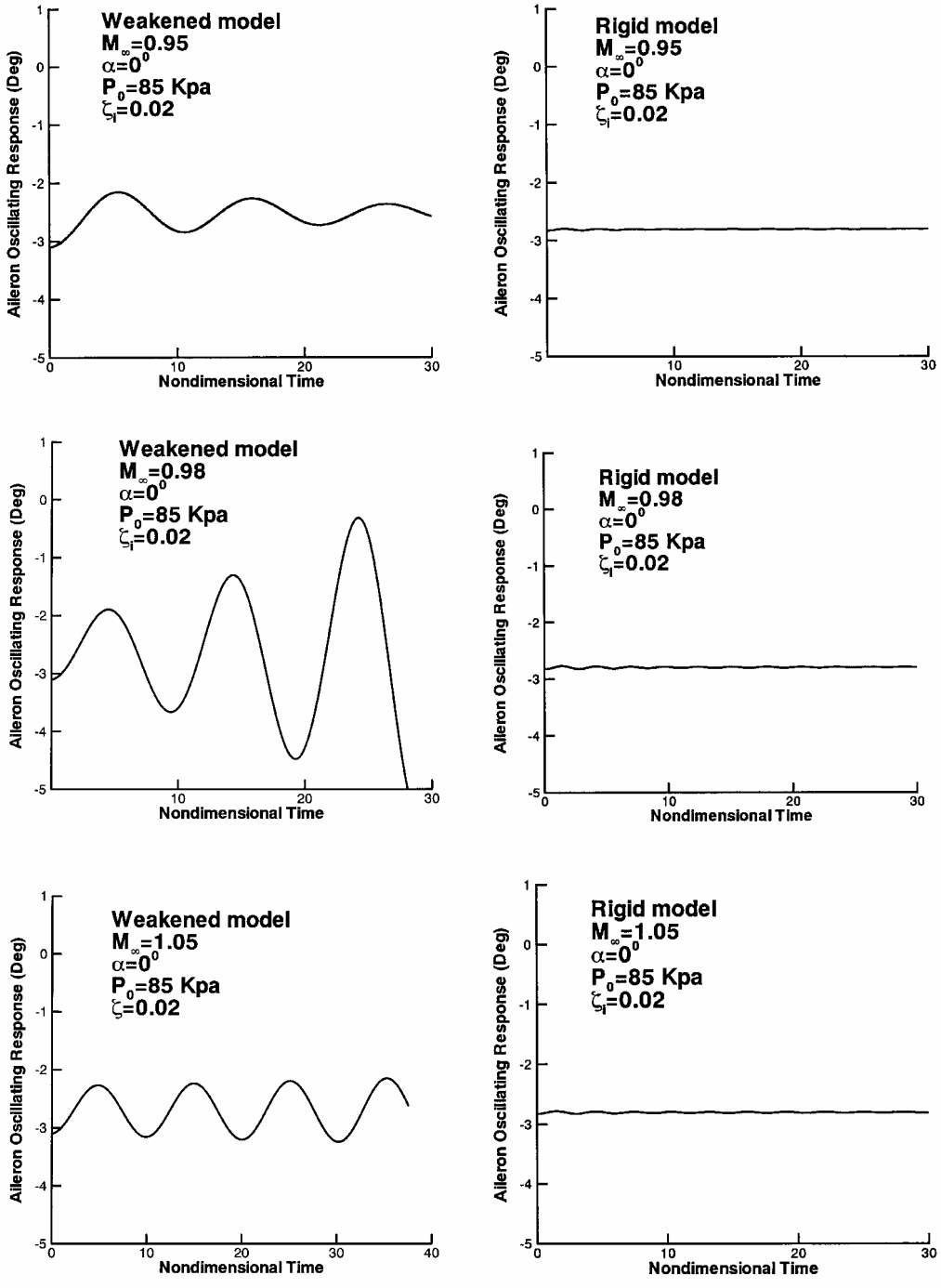

Fig. 12 Dynamic responses of aileron oscillation angle for SST weakened and rigid structural models.

flutter response, not significant enough to explain the discrepancies between the computations and experiment. Their conclusion was that the actual physical conditions in the experiment may not be properly reflected in the computations. Significant changes in flutter speed and frequency could originate in a small difference in Mach numbers in the supersonic flow region. Therefore, any small experimental error in Mach number could lead to significant differences between computed and experimental flutter properties.

SST Wing/Fuselage Model

Finally, aileron flutter simulations are performed for two structural models of the supersonic fuselage/wing configuration[1] designed by the NAL of Japan at three transonic Mach numbers of 0.95, 0.98, and 1.05 under the fixed total pressure of 85 kPa and angle of attack of 0 deg. In the experimental model, the fuselage and main wing are rigid; however, the aileron is attached to the main wing by a spring with different strengths to simulate the hinge stiffness. Figure 10 shows the first six structural modes and natural frequencies of the weakened structural model. For the weakened structural model, the oscillating mode of aileron has the lowest natural frequency of 30.5 Hz. For another rigid structural model, mode shapes and frequencies are the same as the weakened model except that the oscillating frequency of the aileron is increased to 220.7 Hz. The rigid structural model was tested in the aeroelastic wind tunnel at NAL. Flows are found stable at all Mach numbers. Experiments in the next step wish the nonlinear aeroelastic phenomenon of aileron buzz can appear on the weakened structural model at some Mach numbers.

The aeroelastic calculation starts from the steady flow. The grid resolution was only studied for the steady flow computation (not shown in here). The multiblock and surface grids are shown in Figs. 1 and 2. The number of total grid points for the following calculations

is 834,960. A small modal damping coefficient $\zeta_i = 0.02$ was added in the structural equations of motion to damp the unphysical oscillation of small amplitude. The time-step size is taken as 0.01.

Figure 11 shows the comparison of dynamic responses of first sixth modes for the two structural models. For the weakened structural model, the dominant mode is the aileron oscillation mode, which is stable at Mach number of 0.95, but diverges at Mach numbers of 0.98 and 1.05. For the rigid structural model, the dominant mode is the bending mode of wing, which has the small amplitude of oscillation and decays in time for all of the three Mach numbers. The response of the aileron oscillation mode corresponds to the third mode, which does not produce any significant effect on the dominant mode. The responses of aileron oscillation shown in Fig. 12 can further verify the explanation. For the weakened structural model, the amplitude of the aileron oscillation becomes larger and larger until the calculation breaks down due to the use of a simple sheared grid deformation for the aileron deflection. However, for the rigid structural model, the largest amplitude of oscillating angle is only about 0.03 deg, and the responses tend to be stable.

The effects of structural damping have been investigated. Here, only the dynamic responses at Mach number of 0.98 are shown in Fig. 13. The coordinate scale of responses of the rigid model has been amplified. For the weakened structural model, although the amplitude of responses becomes a little larger without structural damping, $\zeta_i = 0$, the flow stability is unchanged. For the rigid structural model, the structural damping has a relatively large effect

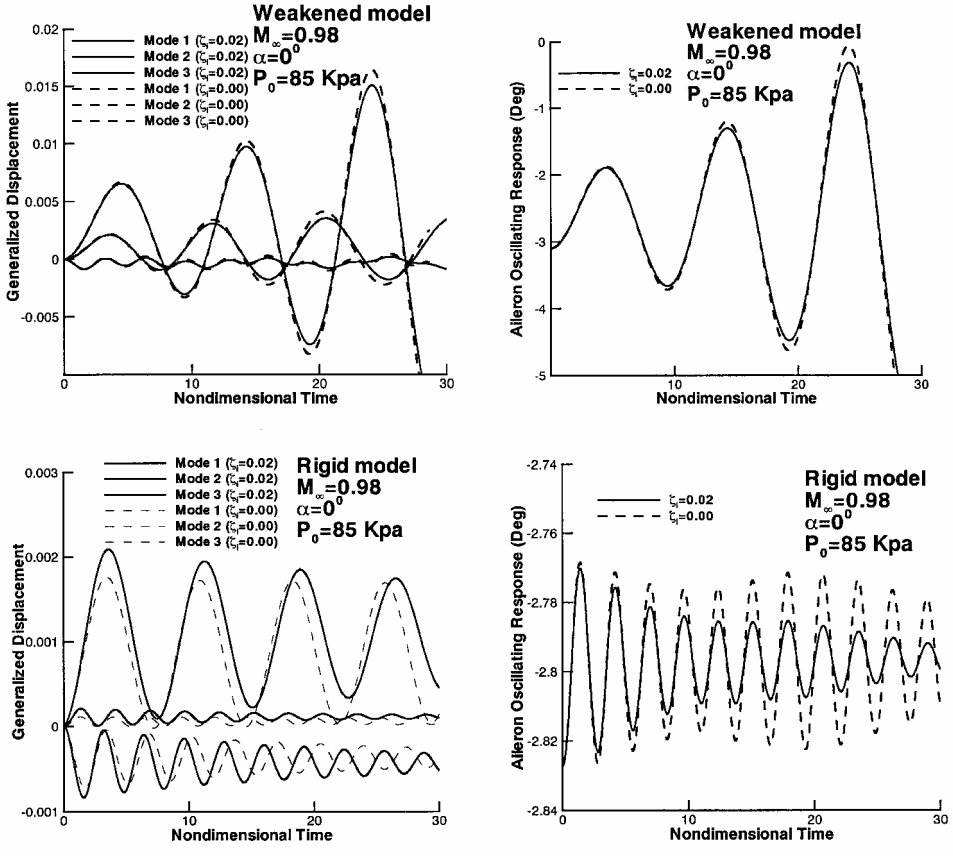

Fig. 13 Effects of structural damping on dynamic responses of modes and aileron oscillation.

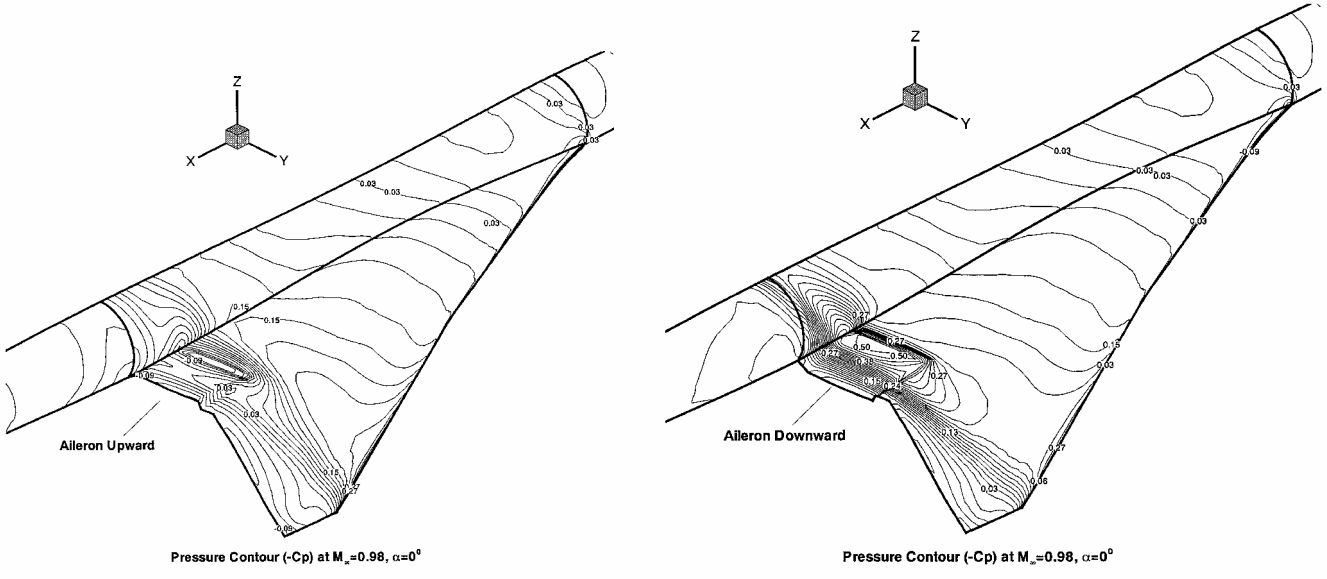

Fig. 14 Pressure contours of aileron oscillation for the weakened structural model at $M_\infty = 0.98$ and $\alpha = 0$ deg.

on the dynamic responses. Even the largest amplitude of aileron oscillation is smaller than 0.03 deg; the oscillation appears to be nonlinear and tends to be neutral without structural damping. Because structural damping always exists in the practical aeroelastic phenomenon, for the dynamic response of small amplitude, a small damping coefficient may be added to damp the unphysical oscillation.

The pressure contours for the weakened structural model at Mach number of 0.98 are shown in Fig. 14, which corresponds two typical positions of aileron oscillation. On the upper surface of the wing, the shock wave becomes weaker as the aileron oscillates upward and becomes stronger as the aileron deflects downward, and the flow behaves just contrary on the lower surface of the wing. Corresponding to general theoretical analysis, the flow instability referred to as aileron buzz is induced by a stronger shock alternately moving on the upper and lower surfaces of wing.

VII. Conclusions

A fully implicit aeroelastic solver has been developed for flutter simulation of complex configuration through the tightly coupled solution of the Navier–Stokes equations and the structural equations of motion. Navier–Stokes equations are discretized with a LU-SGS subiteration algorithm and the modified HLLEW scheme. Structural equations of motion are discretized directly by a second order scheme with subiteration in generalized coordinates. Multiblock grid deformation is performed with the TFI method. IPS and the principle of virtual work are used for data transformation of deformation and force between the fluids and the structures. Three aerodynamic models, the rigid pitching LANN wing, the AGARD 445.6 standard aeroelastic wing, and the aileron flutter models of SST, have been simulated with the present solver. Some useful conclusions are summarized here.

1) Rigid unsteady flow can be solved with attached and deforming grids to validate the grid deformation method. However, for the deforming grid, the transformed matrix had to be calculated at each time step and the geometric conservation law should be considered because the cell volume changes in time.

2) For the multiblock aeroelastic calculation, the tightly coupled method is very important not only for eliminating the lagged flowfield induced by lagged multiblock boundary condition but also for removing the sequencing effects between the fluid and structure.

3) The predictions of flutter speed and frequency for the AGARD 445.6 wing agree well with experimental data in the subsonic and transonic ranges. However, at the supersonic range, the present calculations overpredict the experimental flutter speed and frequency, similar to other computations.

4) For the SST weakened structural model, the phenomenon of aileron buzz has been simulated at the Mach numbers of 0.98 and 1.05, which is induced by the movement of the shock wave alternately on the upper and lower surfaces. For the SST rigid structural model, the flow is stable at all calculated Mach numbers as observed in experiment.

5) Small structural damping may be added to damp the unphysical oscillation of small amplitude when dynamic response is nonlinear or neutral.

References

[1]Sakata, K., "Supersonic Experimental Airplane Program in NAL and Its CFD-Design Research Demand," *Proceedings of the 2nd International CFD Workshop for Super-Sonic Transport Design*, Tokyo, Japan, July 2000, pp. 53–56.

[2]Guruswamy, G. P., "Vortical Flow Computations on Swept Flexible Wings Using Navier–Stokes Equations," *AIAA Journal*, Vol. 28, No. 12, 1990, pp. 2077–2084.

[3]Lee-Rausch, E. M., and Batina, J. T., "Wing Flutter Computations Using an Aeroelastic Model Based on the Navier–Stokes Equations," *Journal of Aircraft*, Vol. 33, No. 6, 1996, pp. 1139–1147.

[4]Goodwin, S. A., Weed, R. A., Sankar, L. N., and Raj, P., "Toward Cost-Effective Aeroelastic Analysis on Advanced Parallel Computing Systems," *Journal of Aircraft*, Vol. 36, No. 4, 1999, pp. 710–715.

[5]Hartwich, P. M., Dobbs, S. K., Arslan, A. E., and Kan, S. C., "Navier–Stokes Computations of Limit-Cycle Oscillations for a B-1-Like Configuration," *Journal of Aircraft*, Vol. 38, No. 2, 2001, pp. 239–247.

[6]Alonso, J. J., and Jameson, A., "Fully-Implicit Time-Marching Aeroelastic Solutions," AIAA Paper 94-0056, Jan. 1994.

[7]Liu, F., Cai, J., Zhu, Y., Tsai, H. M., and Wong, A. S. F., "Calculation of Wing Flutter by a Coupled Fluid–Structure Method," *Journal of Aircraft*, Vol. 38, No. 2, 2001, pp. 334–242.

[8]Goura, G. S. L., Badcock, K. J., Woodgate, M. A., and Richards, B. E., "Implicit Method for the Time Marching Analysis of Flutter," *Aeronautical Journal*, Vol. 105, No. 4, April 2001, pp. 199–214.

[9]Melville, R. B., Morton, S. A., and Rizzetta, D. P., "Implementation of a Fully-Implicit, Aeroelastic Navier–Stokes Solver," AIAA Paper 97-2039, June 1997.

[10]Gordiner, R. E., and Melville, R. B., "Transonic Flutter Simulations Using an Implicit Aeroelastic Solver," *Journal of Aircraft*, Vol. 37, No. 5, 2000, pp. 872–879.

[11]Potsdam, M. A., and Guruswamy, G. P., "A Parallel Multiblock Mesh Movement Scheme for Complex Aeroelastic Applications," AIAA Paper 2001-0716, July 2001.

[12]Wong, A. S. F., Tsai, H. M., Cai, J., Zhu, Y., and Liu, F., "Unsteady Flow Calculations with a Multi-Block Moving Mesh Algorithm," AIAA Paper 2000-1002, Jan. 2000.

[13]Harder, R. L., and Desmarais, R. N., "Interpolation Using Surface Splines," *Journal of Aircraft*, Vol. 9, No. 2, 1972, pp. 189–191.

[14]Appa, K., "Finite-Surface Spline," *Journal of Aircraft*, Vol. 26, No. 5, 1989, pp. 495–496.

[15]Goura, G. S. L., Badcock, K. J., Woodgate, M. A., and Richards, B. E., "A Data Exchange Method for Fluid–Structure Interaction Problems," *Aeronautical Journal*, Vol. 105, No. 4, April 2001, pp. 215–221.

[16]Yang, G. W., and Obayashi, S., "Transonic Aeroelastic Calculation with Full Implicit Subiteration and Deforming Grid Approach," *Proceedings of Aeronautical Numerical Simulation Technology Symposium 2001*, Tokyo, Japan, June 2001.

[17]Thomas, P. D., and Lombard, C. K., "Geometric Conservation Law and Its Application to Flow Computations on Moving Grids," *AIAA Journal*, Vol. 17, No. 10, 1979, pp. 1030–1037.

[18]Yoon, S., and Jameson, A., "Lower–Upper Symmetric–Gauss-Seidel Method for the Euler and Navier–Stokes Equations," *AIAA Journal*, Vol. 26, No. 9, 1988, pp. 1025, 1026.

[19]Obayashi, S., and Guruswamy, G. P., "Convergence Acceleration of a Navier–Stokes Solver for Efficient Static Aeroelastic Computations," *AIAA Journal*, Vol. 33, No. 6, 1995, pp. 1134–1141.

[20]Rizzetta, D. P., and Visbal, M. R., "Comparative Numerical Study of Two Turbulence Models for Airfoil Static and Dynamic Stall," *AIAA Journal*, Vol. 31, No. 4, 1993, pp. 784–786.

[21]Soni, B. K., "Two- and Three-Dimensional Grid Generation for Internal Flow Applications of Computational Fluid Dynamics," AIAA Paper 85-1526, May 1985.

[22]Higenstock, A., "A Fast Method for the Elliptic Generation of Three Dimensional Grids with Full Boundary Control," *Proceedings of Numerical Grid Generation in Computational Fluid Mechanics '88*, Swansea, Wales, 1988, pp. 137–146.

[23]Zwaan, R., "LANN Wing Pitching Oscillation," AGARD-R-702, Aug. 1988.

[24]Yates, E. C., Jr., "AGARD Standard Aeroelastic Configurations for Dynamic Response I-Wing 445.6," AGARD-R-765, July 1988.